WILEY

RESEARCH ARTICLE

Large-eddy simulations of the evolution of imposed turbulence in forced boundary layers in a very long domain

Ola Eriksson[1] | Karl Nilsson[1] | Simon-Philippe Breton[1,2] | Stefan Ivanell[1]

[1]Department of Earth Sciences, Wind Energy Campus Gotland, Uppsala University, Visby, Sweden

[2]Environment and Climate Change Canada, Dorval, Québec, Canada

Correspondence
Ola Eriksson, Department of Earth Sciences, Wind Energy Campus Gotland, Uppsala University, Visby 621 67, Sweden.
Email: ola.eriksson@geo.uu.se

Abstract

The technique of using imposed turbulence in combination with a forced boundary layer in order to model the atmospheric boundary layer is analyzed for a very long domain using large-eddy simulations with different combinations of prescribed velocity profiles and pregenerated turbulence fields based on the Mann model. The ambient flow is first studied in the absence of wind turbines. The velocity profiles undergo a transition throughout the domain with a velocity increase of 10% to 15% close to the ground far downstream in the domain. The turbulence characteristics close to the turbulence plane are, as expected, similar to those of the added Mann turbulence. The turbulence will then undergo a transition throughout the domain to finally reach a balance with the shear profile at a certain downstream distance. This distance is found to depend on the turbulence level of the added Mann turbulence planes. A lower Mann turbulence level generally results in a shorter "balancing" distance. Secondly, a row of 10 turbines is imposed in the simulations at different distances from the plane of turbulence in order to determine how the distance affects wake conditions and power production levels. Our results show that a "balancing" distance is needed between the turbulence plane and the first turbine in the row in order to ensure nonchanging ambient conditions throughout the turbine row. This introduces an increase in the computational costs. The computational cost for the forced boundary technique is normally lower compared with using precursor simulations, for longer domains; however, this needs to be verified further.

KEYWORDS

FBL, forced boundary layer, imposed Mann turbulence, LES, long distance wake

1 | INTRODUCTION

When simulating wind turbines and wind farms, it is important to be able to mimic the atmospheric conditions as accurately as possible and to be aware of the limitations of the selected methods. Large-eddy simulations (LES) can be used to resolve the turbulent scales containing the most energy but are computationally demanding. Today, the computational capacity is much larger than a few years ago; however, it is still very challenging to accurately simulate wind farms in atmospheric conditions. Breton et al[1] provided an overview of the use of LES to perform high-fidelity simulations of wind farms with a focus on available methods for rotor modeling as well as including the relevant characteristics of the atmosphere.

The first problem is that a full calculation including wind turbines needs to take into account many orders of magnitudes of length and time scales, stretching from the scales found at the boundary layer of the turbine blade to atmospheric scales. To limit the problem with the need of high resolution for the boundary layer of the turbine blade, Sørensen et al[2] introduced the concept of actuator lines (ACLs) where body forces represent the blades and thereby reduce the number of grid points needed to represent the blades. The local flow around the turbines can be further simplified by using an actuator disc (ACD) method.[3,4] Porté-Agel et al[5] studied the wake conditions after a single turbine, which was parameterized either using a constantly loaded ACD, an ACD using airfoil data (which induces wake rotation), or an ACL using airfoil data. The main conclusion was that the simulations were in good agreement with measurements (of velocity deficit and turbulence intensity) if

turbine-induced wake rotation was included, which was not the case for the constantly loaded ACD. In this study, therefore, an ACD using airfoil data (which induces wake rotation) is used.

A second consideration is how to include the turbulent atmospheric boundary layer (ABL) conditions as accurately and efficient as possible. It is also important to understand how and to what extent the atmospheric conditions impact the performance of wind farms. When using LES, the atmospheric conditions can either be included by performing a precursor simulation, in which the flow is let to develop using a pressure gradient and a roughness (or some wall model) for the ground, or by forcing the conditions using body forces hereafter referred to as the forced boundary layer (FBL) technique. Wind turbine simulations in ABLs have been performed using LES and a precursor by Churchfield et al,[6] Porté-Agel et al,[5] Calaf et al,[7] and Xie and Archer,[8] among others. performed computations on two aligned turbines parameterized using a flexible ACL model which were imposed in a turbulent atmospheric boundary layer (ABL). The aim of this work was to study the effect of varying the surface roughness and atmospheric stability on power production, structural loads and wake evolution. Calaf et al[7] performed simulations of fully developed flow over a very long array of turbines in a neutral boundary layer. The wind turbines were modeled using a constantly loaded ACD approach. The results from this work showed that the kinetic vertical fluxes were in the same order of magnitude as the power extracted by the wind turbines. Xie and Archer[8] pointed at a classic "overshoot" problem, an overestimation of the mean velocity, near the ground. The FBL technique is a simplified approach to model the ABL was proposed by Mikkelsen et al[9] and Troldborg et al,[10] in which a desired wind profile and synthetic pregenerated turbulence[11,12] were imposed in the computational domain using body forces. By using the FBL technique in combination with imposed turbulence, the required computational time to establish the boundary layer is relatively small and, additionally, any given wind profile and turbulence level can be simulated. Some studies, such as Stevens et al,[13] question how well the FBL technique and imposed turbulence correspond to the turbulent structures of atmospheric conditions. Chivaee and Mickkelsen[14] compared however, with similar setup, a precursor and a FBL technique with the conclusion that the FBL predicted reasonably similar statistics as the precursor around the rotor area. Due to some differences in the used wind shears, some differences were seen above the rotor height. The FBL technique has successfully been combined with the ACD method and has shown to be time efficient and accurate tools for wind turbine production predictions and wake flow simulations. The FBL/ACD technique was used in farm scale simulations in Ivanell et al, [15] Ivanell,[16] and Nilsson et al,[17] where the emphasis was on power predictions. Ivanell et al [15] and Ivanell[16] performed LES/ACD computations of the Horns Rev (HR) wind farm with relatively good agreement in terms of power production compared with measurements. Nilsson et al[17] performed LES/ACD computations of the Lillgrund wind farm with a good (better compared with HR) agreement with measurements in terms of power production, both in terms of trends and levels. The wind farm size in the Lillgrund case is approximately 2000 to 2800 m. Compared with some other wind farms (eg, the Horns Rev wind farm, which is in the order of 5000 m), Lillgrund is a relatively short wind farm. The FBL technique is found to accurately predict power production for short farms, but for cases with longer distances, it has not been thoroughly evaluated. Performance of an in-depth study on how the technique behaves for long wind farms is therefore very interesting. The evolution of turbulence in long lines of wind turbines has been the subject of research in Andersen et al[18] and in Breton et al.[19] In Andersen et al,[18] an infinite row of turbines was simulated using periodic boundary conditions at the inlet and outlet. The turbines were in this case parameterized using the ACL method. This study was performed without using an atmospheric boundary layer and thus studied the turbulence produced by the turbines themselves. In Breton et al,[19] a row of 10 turbines was imposed in uniform conditions both with and without using pregenerated synthetic Mann turbulence. The turbines in this study were parameterized using the ACD method. In this work, the wake flow was characterized, and the power output of the individual turbines was determined. This study concluded that a nearly asymptotic behavior of the flow was achieved far downstream in the row of turbines. Troldborg et al[20] showed however in a study, using the FBL/ACL technique to study the wake interaction between two turbines in different inflow conditions, that the ambient turbulence has a significant impact on the wake interaction and rotor loads.

Works using the FBL technique have been performed by Troldborg et al[21] and Keck et al[22] to study the downstream development of the turbulence. The correlation between the imposed wind profile and the atmospheric turbulence was investigated in Troldborg et al,[21] and it was shown that imposed turbulence was sustained to a large extent throughout the computational domain if a linear wind profile, equal to that used in the Mann model, was also used in the LES. In Keck et al,[22] a wind profile defined by the power law was used, and it was shown that the turbulence approached equilibrium with the wind shear profile when progressing downstream. These works only investigated flow conditions in relatively short domains, and based on the results from these, it is difficult to draw any conclusions on how conditions are developed for longer domains of the size of a wind farm or even wind farm clusters. Therefore, there are still uncertainties in how the model behaves in long domains.

The aim of the study is to further improve the knowledge of how to mimic the atmospheric boundary layer using LES combined with the FBL technique. The study analyzes how the turbulent flow varies as it progresses downstream in a long domain in the absence of wind turbines in a first step. In a second step, a row of 10 turbines is imposed at different downstream positions in the domain and power production and wake conditions are analyzed with the aim of determining how they depend on the distance between the first turbine in the row and the position where the Mann turbulence is imposed. The current work is a continuation of the work in Breton et al.[19] The novelty is that an FBL is introduced. The current work also complement the work by Troldborg et al[21] and Keck et al[22] in terms of the length of studied distances.

The conclusions from the current study can be used to help model very long wind farms using the FBL technique. Also, they can be used to indicate if the FBL/ACD model is suitable for simulating farm wakes and farm-farm interactions, which both deal with flows traveling very long distances. The results can further be used to find needs for improvements in the application of the FBL technique for long distances.

2 | TURBINE SPECIFICATIONS

The turbine used in the current study is comparable with the Vestas V80 turbine from the Horns Rev wind farm. While the real turbine data are unavailable, a downscaling, as described below, of a known turbine is performed based on the same principle as used in Nilsson et al.[17] The turbine in the current study is a downscaled version of the conceptual NREL 5-MW turbine.[23] The downscaled turbine has a smaller nominal power (P = 2 MW) and radius (R = 40 m) compared with the full NREL turbine (5 MW, 63 m). The lift and drag data are exactly the same as in JonkmanJ et al.[23] The chord and twist distributions as functions of the local blade radius used in this study are depicted in Figure 1.

These distributions are determined using a linear downscaling of the blade of the full NREL turbine, and the scaling parameter is the ratio between the radius of the Vestas V80 turbine and the NREL 5-MW turbine.

The downscaled NREL turbine is compared with the Vestas V80 turbine in terms of thrust coefficient, C_T, and electrical power, P_{el}, which are depicted in Figure 2 as functions of the free stream velocity, U_0. The general agreement between the different turbines is good, especially in the region around $U_0 = 8 m/s$ for which this study is performed.

The power output of the turbines is in the current study controlled using a torque-based controller, as described in Nilsson.[24] Briefly, the controller makes use of the aerodynamic torque, M_{aero}, computed by the ACD method, and the generator torque, M_{gen}, which is tabulated as a function of the rotor RPM (see Figure 3). The generator torque curve is created based on the principle described in Jonkman et al[23] and the RPM and torque values defining the start and the end of the different regions are taken from Churchfield.[25]

The production (P) is calculated, according to Equation (1), as the angular velocity of the rotor (Ω_{rotor}) times the aerodynamic torque, M_{aero}.

$$P = \Omega_{rotor} \cdot M_{aero} \tag{1}$$

3 | NUMERICAL MODEL

The simulations are performed with the EllipSys3D code originally developed by Michelsen[26,27] and Sørensen[28] at DTU/Risø. The EllipSys3D code is a general purpose 3D solver based on a finite volume discretization of the Navier-Stokes equations in general curvilinear coordinates and
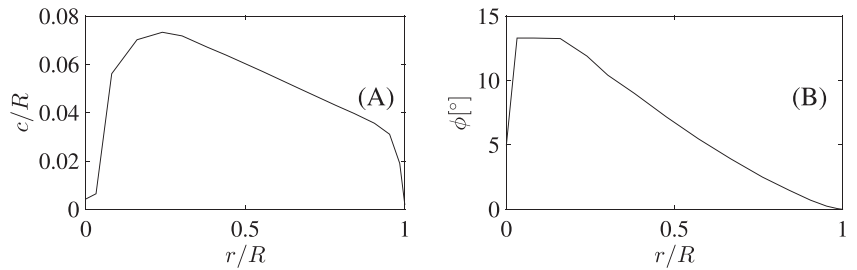

FIGURE 1 (A) Chord (c) and (B) twist distributions (ϕ) as functions of the radial position (r) on the turbine disc with the rotor radius (R)
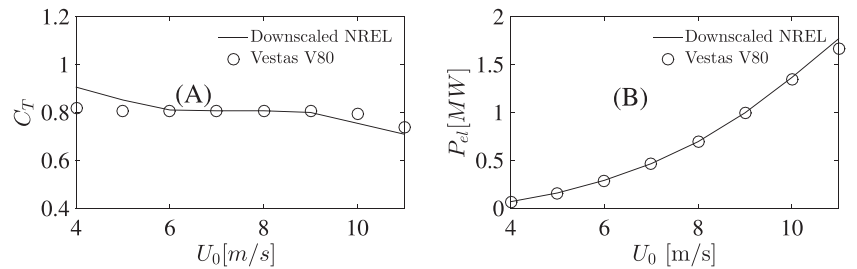

FIGURE 2 (A) The thrust coefficient (C_T) and (B) the electrical power (P_{el}) as functions of the free stream velocity (U_0)
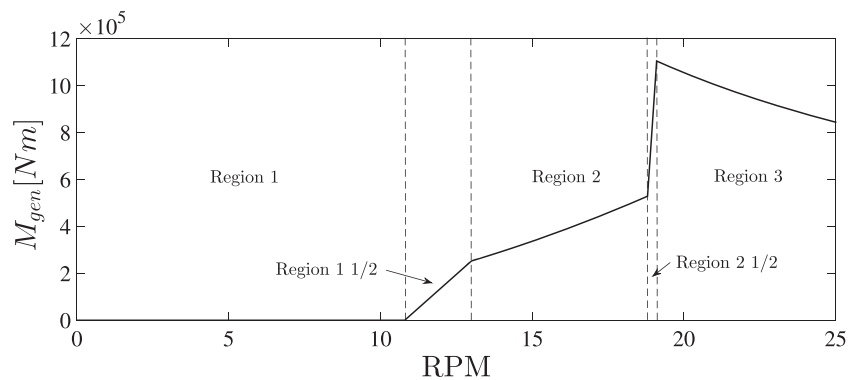

FIGURE 3 Generator torque (M_{gen}) as function of rotational velocity of rotor (RPM) for the wind turbine used in this work
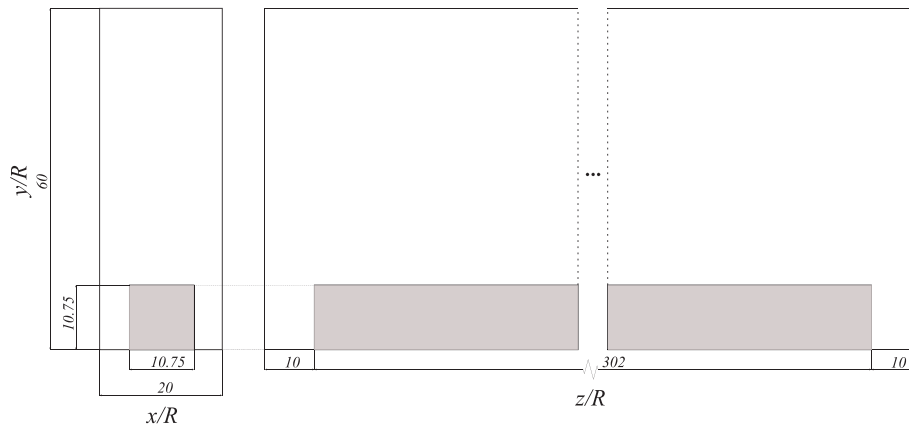
FIGURE 4 Grid architecture for lateral-vertical (left) and streamwise-vertical (right) cross sections. Lengths are normalized with the rotor radius (R) [Colour figure can be viewed at wileyonlinelibrary.com]

is parallelized using a message passing interface (MPI). It is formulated in primitive variables, ie, pressure and velocity, in a collocated storage arrangement. The numerical method uses a blend of a third-order Quadratic Upwind Interpolation for Convective Kinematics (QUICK) scheme (10%) and a fourth-order Central Differences Scheme (CDS) (90%) for the convective terms, while it uses a second-order CDS for the remaining terms. The usage of the blend is a compromise between avoiding nonphysical numerical wiggles and limiting numerical diffusion. The pressure correction equation is based on the Semi-Implicit Method for Pressure-Linked Equations (SIMPLE) algorithm. The numerical model has been described, used, and validated by previous works,[4,15,20,29,30] among others.

The computations are carried out as LES. With the LES technique, large eddies are resolved explicitly and eddies smaller than a certain size are filtered out and modeled by an eddy viscosity–based subgrid scale (SGS) model. For this work, the mixed scale model developed by Ta Phuoc[31] is used in order to ensure similar conditions as in the work by Breton et al.[19] For more information about the LES technique and the SGS models, the reader is referred to Ta Phuoc[31] and Sagaut.[32]

3.1 | Grid, time step, and boundary conditions

The extent of the grid used, as shown in Figure 4, is $322R \times 20R \times 60R$, in the axial ($z$), transversal ($x$), and vertical ($y$) directions, respectively. The corresponding vector for the mean velocities is $U = (W, U, V)$. An inner equidistant region measuring $302R \times 10.75R \times 10.75R$ with a resolution of $\Delta x = 0.1R$ is used. This value is based on experience from previous studies.[16,17,19] Outside of the equidistant region, the grid is stretched towards all boundaries. The grid is defined using 192 blocks (for parallelization purposes) with 64^3 grid points each, resulting in approximately $5.0 \cdot 10^7$ grid points in total.

A no-slip condition is imposed at the bottom boundary, a constant velocity is imposed at the top boundary, and cyclic conditions are used at the lateral boundaries. A Dirichlet condition is imposed for velocities and pressure at the inlet and a convective condition (a zero second-order derivative) is imposed at the outlet.

The size of the simulation time step, Δt, is determined as to fulfill the Courant-Friedrichs-Lewy (CFL) condition,

$$CFL = \frac{U_0 \Delta t}{\Delta x} < 1. \tag{2}$$

Δt is set to $0.025R/U_0$ resulting in a CFL number equal to 0.25 based on the mean streamwise velocity at hub height. The CFL value is chosen conservatively in order to take local effects from velocity fluctuations, which results in higher velocities compared with U_0, and wind shear profile into account.

3.2 | Turbine modeling

The turbines are modeled in the simulations using the ACD method, described by Mikkelsen[4] and Troldborg et al.[33] In the ACD method, the rotor is modeled using body forces that are determined through a blade element approach combined with tabulated airfoil data (lift and drag coefficients, C_L and C_D, as functions of the angle of attack). The main idea is to compute the flow over the rotor disc without the need to resolve the boundary layer on the blades. In order to avoid numerical problems, the body forces are smeared in the axial direction using a one-dimensional Gaussian approach with a smearing factor, $\epsilon = 0.2R$, a value based on experience from previous studies (see Ivanell et al[30]). The rotor disc is discretized using a local polar grid with 21 grid points along the radial direction and 81 points in the azimuthal direction.

3.3 | Forced boundary layer

The wind shear is imposed and preserved in the domain by means of body forces according to a methodology described in Troldborg et al.[21] This procedure is performed by initially applying relatively small body forces everywhere in the domain. The results from this simulation are saved
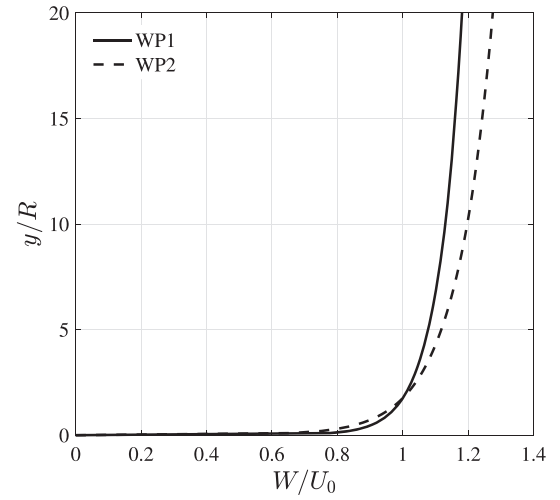
FIGURE 5 Wind profiles normalized with the free stream velocity (U_0) and the rotor radius (R)

TABLE 1 The turbulence boxes (M1, M2, M3) are based on different roughness lengths (z_0)

Turbulence Box	M1	M2	M3
z_0	10^{-6} m	10^{-4} m	10^{-2} m

and used as an initial flow field for simulations including atmospheric turbulence and wind turbines. The surface conditions are included in the simulations by the shape of the wind shear that is imposed.

In this work, two different wind profiles are used, as depicted in Figure 5. These are defined according to the logarithmic law,

$$W(y) = \frac{u_\star}{\kappa} ln(y/z_0), \tag{3}$$

where $\kappa = 0.40$ is the von Kármán constant, z_0 is the roughness length, and $u_\star$ is the friction velocity which is determined by

$$u_\star = \frac{U_0 \kappa}{ln(y_{hub}/z_0)}, \tag{4}$$

where $y_{hub} = 1.75R$ is the hub height. The first profile used in this study is named WP1 and is defined using $z_0 = 10^{-4}$m, which is a typical value for offshore. For comparison, a second profile, WP2, is defined using $z_0 = 10^{-2}$m; this value correspond rather to an open flat area onshore.

3.4 | Imposed turbulence

Synthetic atmospheric turbulence is generated using the Mann model.[11,12] The turbulent field computed by this model is homogeneous, Gaussian, anisotropic, and has the same second order statistics as neutral atmospheric turbulence. The pre-generated turbulence created by the Mann model can be adjusted by a linear shear profile. This profile is defined using certain values of z_0, U_0, and y_h. U_0 and y_h are in the current case kept constant, so the main parameter to influence the shear and thus the turbulence characteristics is z_0. A fit is made to the three velocity components and the cross spectra of a given one point turbulence spectrum to determine the energy dissipation factor $\alpha\epsilon^{2/3}$ (here, z_0 is used as the scaling factor), length scale L, and anisotropy factor Γ, that are used in the Mann algorithm.

In the present study, three different turbulence boxes all fitted to the Kaimal spectrum are created in which z_0 is set according to Table 1. The outcome of the model is a box measuring $120R \times 25R \times 25R$ with a resolution (which is equidistant throughout the box) of approximately $0.12R \times 0.19R \times 0.19R$. The box consists of $1024 \times 128 \times 128$ grid points. As the box is periodic in all directions, only a quarter of the xy-plane is used in the LES to avoid spanwise periodicity in the turbulence, resulting in a box measuring $120R \times 12.5R \times 12.5R$ with $1024 \times 64 \times 64$ grid points.

The box is divided into 1024 xy-planes, one for each grid point in the axial direction in the Mann box. By assuming the Taylor frozen turbulence hypothesis, each of these planes consist of a time step. The fluctuations in these planes are then recalculated into body forces, and the planes are imposed in the computational domain with its lower right corner positioned at $(z, x, y) = (L_{MANN}, 3.75R, 0.4R)$, where $L_{MANN} = 13R$. Similarly to the ACD method, the body forces are smeared in the axial direction in order to avoid numerical problems. For a more detailed description about the procedure on how to recalculate the fluctuations into body forces, the reader is referred to Troldborg et al.[21]

4 | SIMULATION CASES

Six different configurations of the wind profile and the atmospheric turbulence are simulated as defined in Table 2. Initially, each of these six cases are simulated in the absence of wind turbines in order to determine how the flow conditions develop in the domain.

Simulation Case	S1	S2	S3	S4	S5	S6
Wind profile	WP1	WP1	WP1	WP2	WP2	WP2
Turbulence box	M1	M2	M3	M1	M2	M3

TABLE 2 The simulation cases (S1-S6) use different combinations of wind profiles (WP1-WP2) and turbulence boxes (M1-M3)
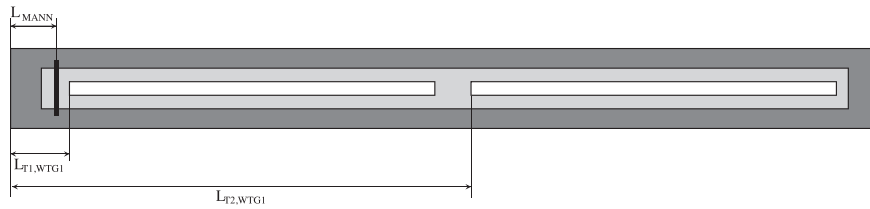

FIGURE 6 Positions seen from above of Mann planes (thick black lines) and turbine rows (white rectangles) for cases T1 and T2. The equidistant and stretched regions of the grid are highlighted in light and dark grey, respectively. The distance from the inlet (L) is marked
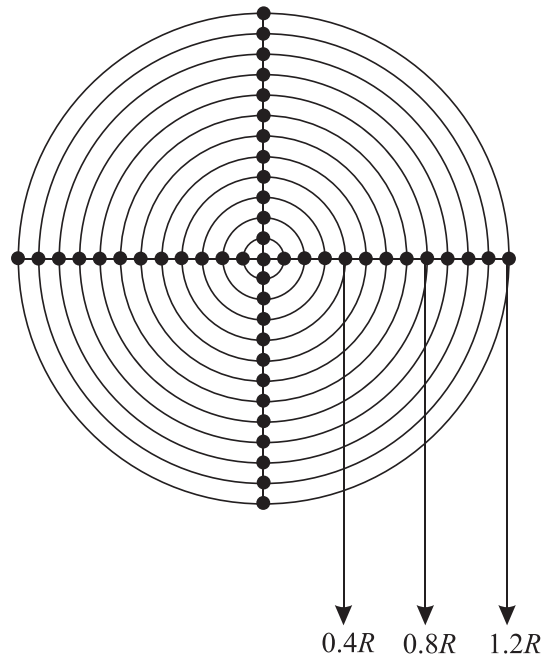

$0.4R$ $0.8R$ $1.2R$

FIGURE 7 A schematical figure (with circles every 0.1 rotor radius R from the center) explaining the probe sheet used for collection of velocity time series. The values are extracted for the marked dots

In the presence of wind turbines, the six cases are simulated for two variations (T1 and T2) of turbine positioning in the domain, as depicted in Figure 6. For these sets of simulations, a single row of 10 turbines is used. The separation distance between the turbines is $14R$ corresponding to the distance separating the turbines in the Horns Rev wind farm in the 270° direction. The turbine rotors are centered at $(z_c, x_c, y_c) = (L_{i,j}, 10R, 1.75R)$, where L is the axial positions of the turbines, $i = T1, T2$ is the set of simulations, and $j = WTG1, WTG2, \ldots, WTG10$ is the number of the turbine in the row. $L_{T1,WTG1} = 17R$ and $L_{T2,WTG1} = 168R$.

In total, 3×6 simulations are performed, each over 50 000 time steps. The first 26 000 time steps are used to establish stationary conditions. The last 24 000 time steps (50 min) are used in the evaluation of the simulation results to get statistically stable results[34] and to have a number of time series to evaluate the spectra over.

4.1 | Analysis methodology

The mean flow conditions in the absence of wind turbines are determined in terms of power spectra, S_z, profile of the mean axial velocity component W, and standard deviation of velocity components σ_i, where $i = z, x, y$.

In order to save time series of velocities at several points of interest, probe sheets are inserted at different z positions. The points on each probe sheet are distributed according to Figure 7 and the center position of each sheet is in (x_c, y_c).

S_z is determined from the streamwise velocity component and is averaged both temporally and spatially. The temporal averaging is performed over the 24 000 time steps used in the evaluation. These are divided into five blocks of 4800 time steps each. Furthermore, the discrete fast Fourier transform is determined for each block, and a temporal average of the five blocks is calculated. In a second step, the spatial average is calculated over the points on the probe sheet defined by $x_c \pm 1.2R$ and $y_c \pm 1.2R$ in the transversal and vertical directions, respectively.

W and σ_i are saved as temporal averages (over the 24 000 time steps) in every point of the full grid. Based on this information and in absence of wind turbines, W and σ_i are averaged for each height in the transversal direction over the region defined by $5R \leq x \leq 15R$.

In the presence of wind turbines, W and σ_z are determined at $7R$ behind each turbine. These are averaged using grid points contained in the region defined by $x_c, y_c \pm 1.2R$ according to Figure 7. The operational characteristics of the turbines are evaluated using the power production,

P, of each individual turbine. Error bars for P are calculated, as the standard deviation divided by the number of samples, based on the five 10-minute periods in the last 50 minutes used in the evaluation.

5 | RESULTS AND DISCUSSION

5.1 | In the absence of wind turbines

Wind profiles of W are extracted at various downstream positions. In Figure 8, the wind profiles for the first part of the domain are shown. Compared with the originally prescribed wind profiles, these will undergo a transition throughout the domain. However, for larger downstream distances, the wind profiles, as observed in Figure 9, reach a constant shape.

In Figures 8 and 9, only results using the turbulence box M1 were shown. The other turbulence boxes produce similar behavior. The largest deviation compared to the original FBL profile is found close to ground where the offset is around 10-15%, depending on the synthetic turbulence
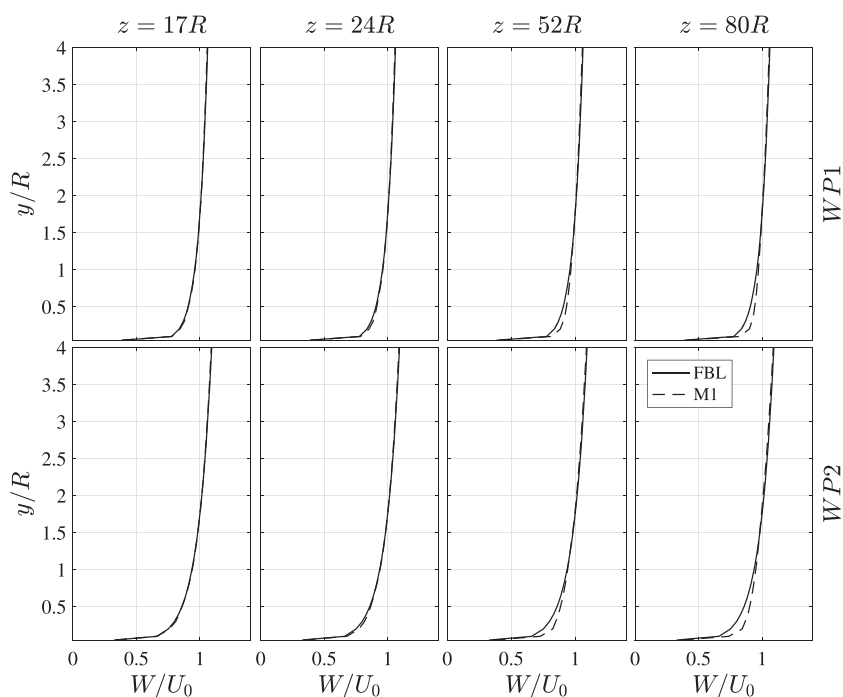

FIGURE 8   Downstream wind profiles (normalized with the free stream velocity [U_0] and the rotor radius [R]) for cases S1 and S4. The originally prescribed wind profile, FBL, is also shown. The figure depicts the lower part of the boundary layer and the first part of the domain
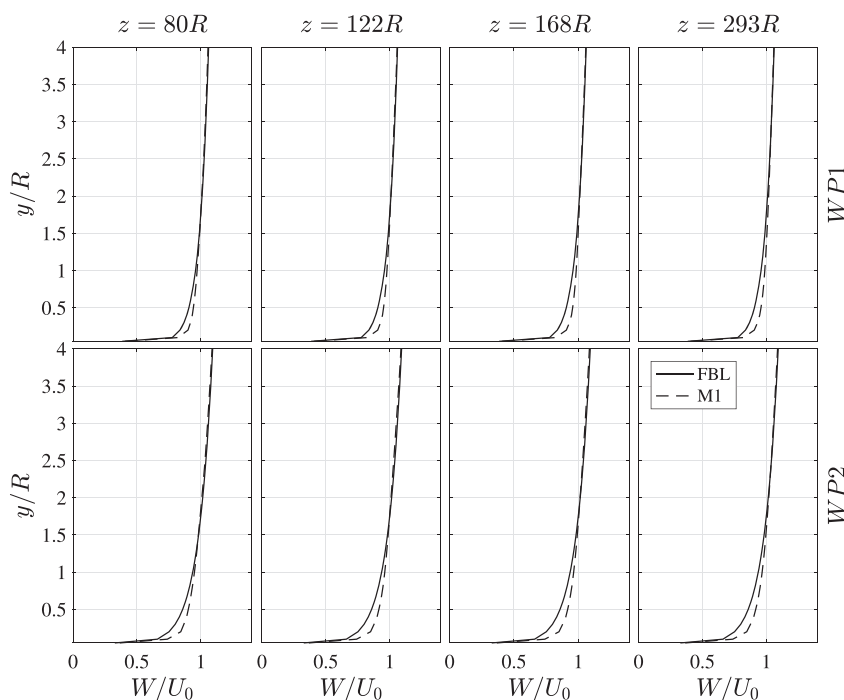
FIGURE 9   Downstream wind profiles (normalized with the free stream velocity [U_0] and the rotor radius [R]) for cases S1 and S4. The originally prescribed wind profile, FBL, is also shown. The figure depicts the lower part of the boundary layer and the second part of the domain

level and the original wind profile. A lower synthetic turbulence level reduces the offset. Also, the wind profile with the lowest z_0 value results in a smaller percental difference.

The deviation from the original profiles is believed to be connected to the interaction of the FBL and the added synthetic turbulence. This issue is to be noted, but possible solutions to limit this behavior are not a focus of this paper and hence will not be elaborated on further. The study of this issue is left for future work.

5.1.1 | Region of distortion

As shown in the current study and as described earlier in Troldborg et al,[21] the Mann turbulence imposed in the domain adds a distortion to the flow field. In Figure 10, σ_i is depicted at y_{hub}. σ_i is initially increasing until a certain downstream position, after which it starts to decay. Figure 8 shows that the wind shear also develops inside this region. The initial growth region for the turbulence is referred to as the region of distortion. The level of the initial growth is dependent on the turbulence level in the Mann box, as seen in Figure 10, where the box with highest turbulence level, M3, renders the highest values of σ_i for a given wind shear and vice versa. Furthermore, in a part of the distortion region directly after the turbulence plane, $\sigma_y > \sigma_x$. For neutral atmospheric turbulence, the inverse relationship is expected.[12] As discussed in Troldborg et al,[21] this can be due to a distortion that occurs because the same mean velocity is assumed across the domain when the Taylor frozen turbulence hypothesis is used.

In Figure 11, S_z is depicted at different downstream positions. As the same trend is found for all simulation cases, only the spectra for case S1 is shown for the sake of conciseness. It is observed that in the distortion region, Figure 11A, energy levels increase with downstream distance in the low- and high-frequency portions of the spectra while the levels are more or less constant for the midrange frequencies. One reason for this, as discussed in Troldborg et al,[21] is that the resolution in the LES is finer compared with that used in the Mann box, allowing smaller scales in the former. Due to the cascade process of turbulence, the high-frequency portion of the turbulence therefore increases in the LES. Another reason is the implementation and smearing of the body forces, as discussed in Keck et al.[22] The increase in the larger scales is believed to be due to the fact that the larger height of the domain compared with the Mann box allows for larger turbulent structures.

5.1.2 | Region of adaptation

After the distortion region, the flow adapts to the imposed shear profile, resulting in a decay of turbulent energy levels. This decay can be seen in S_z, Figure 11B, which reveals a broadband decrease in the energy levels with increased downstream position. Furthermore, this decay can also be seen in Figure 10, where all components of σ_i are decaying with downstream distance. However, it is observed that the decay of σ_i levels out as it progresses downstream. The level of each component far downstream is observed to be dictated by the wind shear profile as the cases using the same wind shear render more or less the same values of σ_i, regardless of the initial Mann box. In the adaptation region, the initial Mann turbulence undergoes a transition towards FBL turbulence, which is in equilibrium with the wind shear. Figure 9 shows that the wind shear inside this region has a constant shape. For turbulence, which is in equilibrium with the wind shear, the lowest value of σ_i is expected to be observed for the smallest wind shear gradient and vice versa. This behavior is observed far downstream in Figure 10, without inconsistencies.
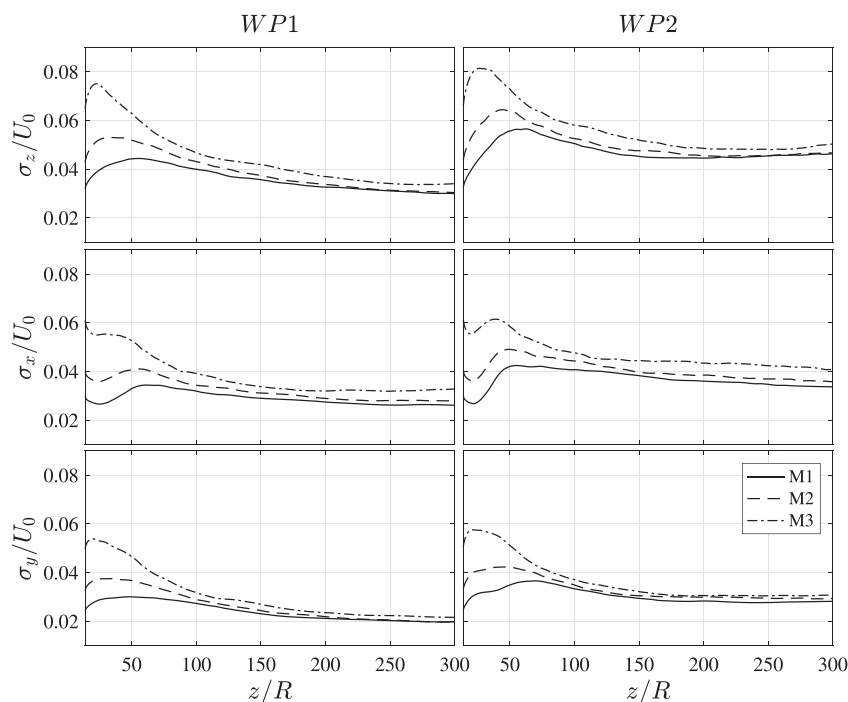

FIGURE 10 Normalized standard deviations at hub height in the absence of wind turbines for different wind profiles and turbulence boxes as a function of the downstream distance normalized with the radius R
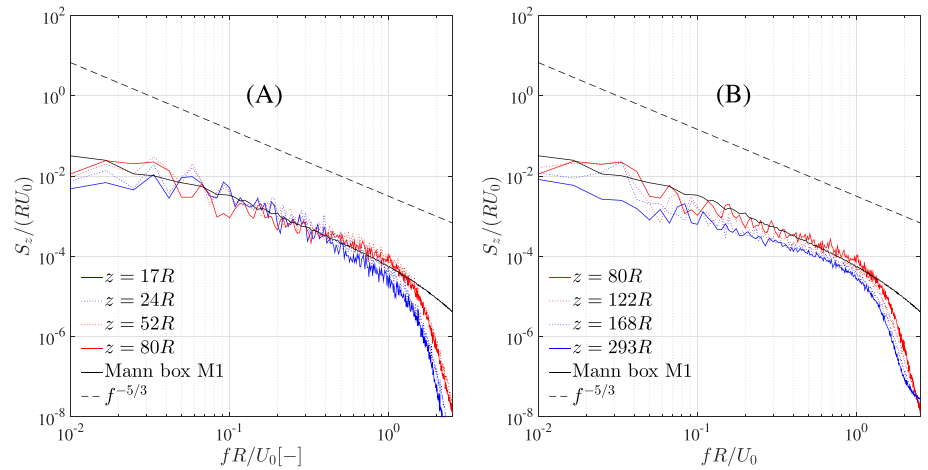
FIGURE 11 Power spectra of fluctuations of axial velocity component for simulation case S1 in the absence of wind turbines for (A) distortion region and (B) adaptation region [Colour figure can be viewed at wileyonlinelibrary.com]
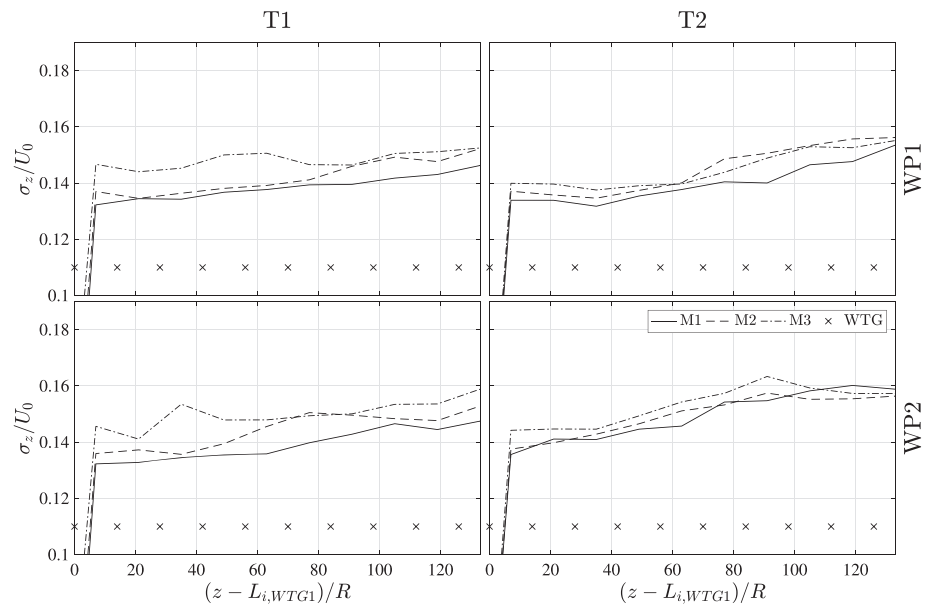

FIGURE 12 Normalized (with the free stream velocity [U_0]) standard deviation of the axial velocity component at hub height as a function of downstream distance (normalized with the radius R) in the presence of turbines, for the two positions of the row of turbines (T1, T2) and two different wind profiles (WP1, WP2). The turbine positions are shown with the x

As a last remark, in the adaptation region, the levels of σ_i are generally observed to satisfy $\sigma_z > \sigma_x > \sigma_y$ for all flow cases, which is expected for neutral atmospheric turbulence.[12]

5.2 | In the presence of wind turbines

When adding wind turbines to the flow, momentum will be extracted from the flow at the disc locations. Furthermore, as shown in Breton et al,[19] the turbulence level in the wake will be increased as compared with the ambient conditions.

The streamwise turbulence level through the row of turbines is shown in Figure 12. In this figure, it is observed that σ_z/U_0 is approximately 0.13 to 0.14 in the beginning of the row of turbines. This value increases slightly and reaches a level of 0.15 to 0.16, depending on the flow case, by the end of the row.

It is observed that, generally, turbulence box M3 renders slightly higher values of σ_z throughout the wake flow compared with when using M2 and M1. However, this difference in σ_z when using the different Mann boxes decreases as the distance between the first turbine in the row and the plane of turbulence for a given wind shear profile increases. This behavior is expected since the importance of the initial turbulence decreases with increased downstream distance.

Studying the development of the mean axial velocity, W, through out the rows in Figure 13, W is found to be in the order of 0.65 U_0 after the first turbine in the row. Furthermore, it is observed that the trend of W coincides with that of σ_z. In fact, as σ_z increases throughout the row of turbines, so does W. This behavior is expected since an elevated σ_z promotes mixing (which promotes the kinetic momentum flux), which, in turn, promotes the recovery of W.

The power production, P, is expected to be directly linked to W in the wake flow. Consequently, as seen studying the relative production in Figure 14, the trends of P are very similar to those of W for the respective flow cases. P is in this case normalized with P_{ref}, which is the production for WTG1, for T1 and for flow case S1.
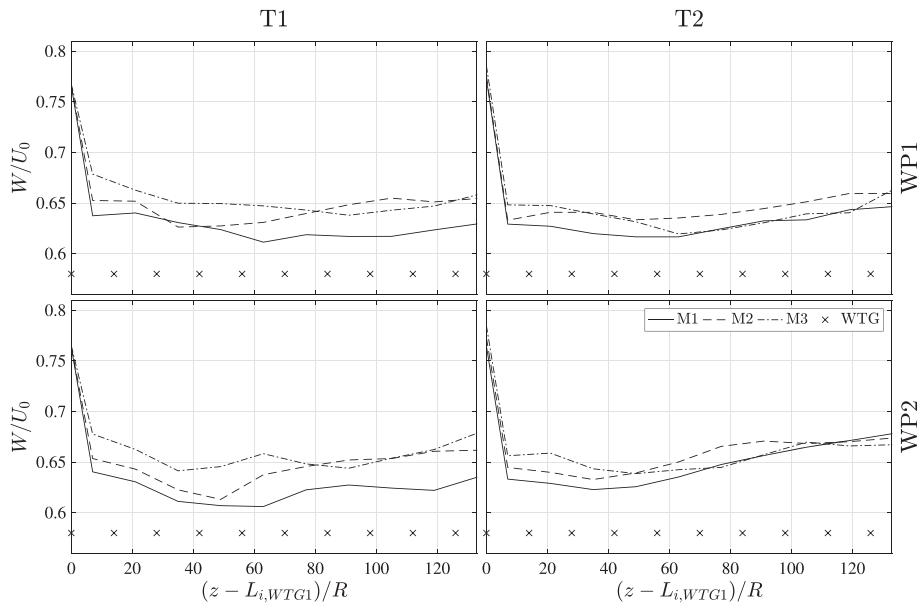
FIGURE 13 Normalized (with the free stream velocity [U_0]) mean axial velocity component at hub height as a function of downstream distance (normalized with the radius R) in the presence of turbines, for the two positions of the row of turbines (T1, T2) and two different wind profiles (WP1, WP2). The turbine positions are shown with the x
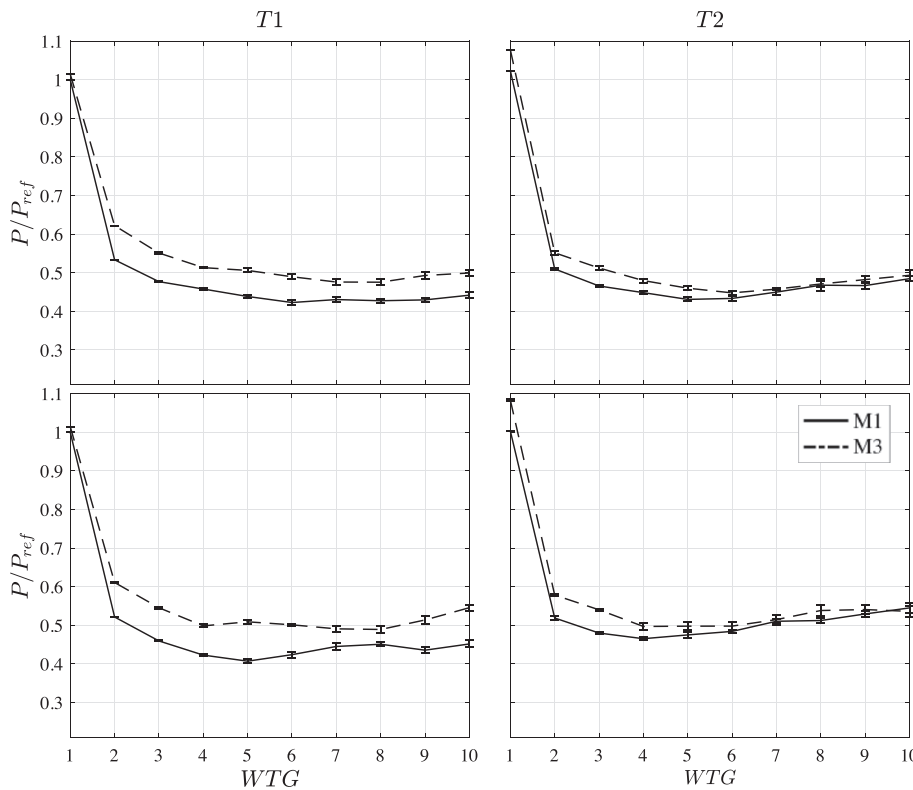

FIGURE 14 Relative power production for the different cases, with two different positions of the row of turbines (T1, T2) and two different wind profiles (WP1, WP2). Error bars show the variation between the five 10-min periods used in the evaluation

For T1, the general trend is that the simulations using M1 give the lowest values of production while the simulations using M3 give the highest. However, there are only marginal differences in P for the different wind profiles for a given turbulence box. Therefore, when imposing the turbines according to case T1, the levels and trends of P are mainly observed to be dictated by the initial turbulence and less by the wind shear. On the other hand, the ambient turbulence level, which was seen in Figure 10, will in such a situation inevitably change with downstream distance in the flow outside of the wake flow, which will affect the production trend.

For T2, the deviations in P when using the different turbulence boxes are small and the trends are different for each wind profile. Therefore, when imposing the turbines according to case T2, the levels and trends of P are observed to be mainly influenced by the FBL turbulence dictated by the wind shear profile and less by the initial turbulence. Attention needs to be paid here, since the Mann turbulence is fitted to atmospheric conditions, which is not necessarily the case with the FBL turbulence that is found far downstream where the turbulence level is in equilibrium with the wind shear.

For distances stretching even further downstream, such as when analyzing farm wakes and farm-farm interaction, the FBL technique seems to be applicable since the turbulence far downstream is found to be in equilibrium with the wind shear profile and does not decay completely. For

the combinations of turbulence and wind shear used in the study, the required distance from the turbulence plane to the first turbine seems to be somewhere around 80R to avoid the development of the ambient conditions to impact the relative production. However, before performing such a study, the recovery rate of the wake flow parameters over large distances needs to be studied further.

6 | CONCLUSIONS

The FBL technique used for modeling the atmospheric boundary layer has been analyzed for a very long domain using LES. For this purpose, two different wind profiles were evaluated in combination with three pregenerated turbulence fields resulting in six simulation cases. First, the six simulation cases were performed in the absence of wind turbines, with the aim of determining the ambient flow conditions. The main findings from these simulations were that, regardless of the characteristics of the imposed pregenerated turbulence, the wind shear profile dictated the ambient conditions at a distance sufficiently far, here around 80R depending on the used wind shear and turbulence, from where the turbulence planes were introduced. In other words, the initial Mann turbulence was found to undergo a transition towards FBL turbulence. It can be noted that the distance needed to reach the FBL turbulence varies and potentially with experience a suitable setup can potentially decrease the distance. Typically, it seems like a lower distance is needed when using a lower level in the imposed pregenerated turbulence.

Second, a row of 10 turbines was imposed in the simulations. The position of the row relative to the plane of turbulence was varied in order to determine how this distance affected wake conditions and power production levels and trends. The simulations also investigated to what extent the shape of the wind shear and the characteristics of the imposed turbulence were affecting the wake flow and power production. It was found that if the row of turbines was placed close to the plane of turbulence, the production of the turbines in the row was mainly affected by the initial turbulence and not the wind shear profile. However, the ambient conditions outside the wake flow, as seen in the simulations without any turbines, are found to change quite drastically throughout the row of turbines. This was also reflected in the production trends. If the turbines are placed far away from the turbulence planes, the initial turbulence is found to be of less importance since the turbines are exposed to FBL turbulence, which is found to be dictated by the wind shear. It can be noted that some development compared with the original wind shear was seen for the first part of the domain; this is related to how the turbulence impact the imposed wind shear.

The forced boundary layer has often been used for simulations with the turbulence plane introduced close to the turbines. This study shows that for long wind farms, a development of the ambient conditions can be seen. However, by placing the turbines further away from the turbulence plane, there the turbulence is in equilibrium with the shear, the development of the ambient conditions is avoided, and the method can be used also for these cases. Also, in real life, the turbulence for neutral atmospheric conditions is shear generated, so the turbulence is "coherent" with the wind shear. The trend of the ambient conditions indicates therefore that the model could be suitable for simulating farm wakes and farm-farm interaction.

The FBL technique used for modeling the atmospheric boundary layer has been analyzed for a very long domain using LES. For short domains, it is expected that computational cost is less using the FBL technique compared with using a precursor. However, for longer domains, taking into account the needed development distance using the FBL technique, the difference in computational time needs to be verified further. Future studies that can indicate suitable setup to decrease the needed development distance is of interest. It was also noted that some development compared wit the original wind shear was seen for the first part of the domain, which was related to how the turbulence impact the imposed wind shear. It is therefore also of interest to further analyse how to decrease this development, adjust the FBL technique to handle this, or change the imposed wind shear to eventually reach the desired wind shear. It can in later studies for long domains also be of interest to consider a wind veer or Coriolis force. Future work of interest is also to include the impact of different atmospheric stabilities

ORCID

Ola Eriksson 🔟 https://orcid.org/0000-0003-2386-1105

REFERENCES

1. Breton S-P, Sumner J, Sørensen J, Hansen K, Sarmast S, Ivanell S. A survey of modelling methods for high-fidelity wind farm simulations using large eddy simulation. *Philos Trans R Soc A Math Phys Eng Sci*. 2017;375:20160097.
2. Sørensen J, Shen W. Numerical modeling of wind turbine wakes. *J Fluids Eng*. 2002;124:393-399.
3. Sørensen J, Myken A. Unsteady actuator disc model for horizontal axis wind turbines. *J Wind Eng Ind Aerodyn*. 1992;39:139-149.
4. Mikkelsen, R. Actuator disc methods applied to wind turbines. *PhD thesis*; 2003.
5. Porté-Agel F, Wu Y-T, Lu H, Conzemius RJ. Large-eddy simulation of atmospheric boundary layer flow through wind turbines and wind farms. *J Wind Eng Ind Aerodyn*. 2011;99:154-168.

6. Churchfield M, Lee S, Michalakes J, Moriarty P. A numerical study of the effects of atmospheric and wake turbulence on wind turbine dynamics. *J Turbul.* 2012;13:N14. https://doi.org/10.1080/14685248.2012.668191

7. Calaf M, Meneveau C, Meyers J. Large eddy simulation study of fully developed wind-turbine array boundary layers. *Phys Fluids.* 2010;22(015110).

8. Xie S, Archer C. Self-similarity and turbulence characteristics of wind turbine wakes via large-eddy simulation. *Wind Energy.* 2015;18:1815-1838.

9. Mikkelsen R, Sørensen JN, Øye S, Troldborg N. Analysis of power enhancement for a row of wind turbines using the actuator line technique. *J Phys Conf Ser.* 2007;75:012,044.

10. Troldborg N, Sørensen JN, Mikkelsen R. Actuator line simulation of wake of wind turbine operating in turbulent inflow. *J Physics: Conf Series.* 2007;75(012063).

11. Mann J. The spatial structure of neutral atmospheric surface-layer turbulence. *J Fluid Mech.* 1994;273:141-168.

12. Mann J. Wind field simulation. *Probab Eng Mech.* 1998;13:269-282.

13. Stevens R, Graham J, Meneveau C. A concurrent precursor inflow method for large eddy simulations and applications to finite length wind farms. *Renew Energy.* 2014;68:46-50.

14. Chivaee H, Mickkelsen R. Comparing wall modeled LES and prescribed boundary layer approach in infinite wind farm simulations. In: 33rd Wind Energy Symposium American Institute of Aeronautics and Astronautics; 2014. https://doi.org/10.2514/6.2015-1470

15. Ivanell S, Mikkelsen R, Sørensen JN, Henningson D. Three-dimensional actuator disc modeling of wind farm wake interaction. In Proc. of the European Wind Energy Conference and ExhibitionEWEA; 2008:1–10.

16. Ivanell S. Numerical computations of wind turbine wakes. *PhD thesis*; 2009.

17. Nilsson K, Ivanell S, Hansen K, Mikkelsen R, Sørensen J, Breton S-P, Henningson D. Large-eddy simulations of the Lillgrund wind farm. *Wind Energy.* 2015;18:449-467.

18. Andersen S., Sørensen J, Mikkelsen R. Simulation of the inherent turbulence and wake interaction inside an infinitely long row of wind turbines. *J Turbul.* 2013;14:1-24.

19. Breton S-P, Nilsson K, Olivares-Espinosa H, Masson C, Dufresne L, Ivanell S. Study of the influence of imposed turbulence on the asymptotic wake deficit in a very long line of wind turbines. *Renew Energy.* 2014;70:153-163.

20. Troldborg N, Larsen GC, Madsen HA, Hansen KS, Sørensen JN, Mikkelsen R. *Numerical Simulations of Wake Interaction Between Two Wind Turbines at Various Inflow Conditions*, Vol. 14; 2011;859-876. Troldborg, Sørensen, Mikkelsen & Sørensen.

21. Troldborg N, Sørensen J, Mikkelsen R, Sørensen N. A simple atmospheric boundary layer model applied to large eddy simulations of wind turbine wakes. *Wind Energy.* 2014;17:657-669.

22. Keck R-E, Mikkelsen R, Troldborg N, de Maré MSH. Synthetic atmospheric turbulence and wind shear in large eddy simulations of wind turbine wakes. *Wind Energy.* 2014;17:1247-1267.

23. Jonkman J, Butterfield S, Musial W, Scott G. Definition of a 5-MW Reference Wind Turbine for Offshore System Development. *Tech. Rep*, NREL; 2009. NREL/TP-500-38060.

24. Nilsson K. *Numerical Computations of Wind Turbine Wakes and Wake Interaction—Optimization and Control.* KTH Engineering Mechanics; 2012.

25. Churchfield M. A method for designing generic wind turbine models representative of real turbines and generic siemens swt-2.3-93 and vestas v80 specifications. *Tech. Rep*, National Renewable Energy Laboratory; 2013.

26. Michelsen JA. Basis3D—A Platform for Development of Multiblock PDE Solvers. *Tech. Rep*, Technical University of Denmark; 1992. AFM 92-05.

27. Michelsen JA. Block Structured Multigrid Solution of 2D and 3D Elliptic PDE's. *Tech Rep*, Technical University of Denmark; 1994. AFM 94-06.

28. Sørensen NN. General purpose flow solver applied to flow over hills. *PhD thesis*; 1995.

29. Troldborg N, Sørensen JN, Mikkelsen R. Numerical simulations of wake characteristics of a wind turbine in uniform inflow. *Wind Energy.* 2010;13:86-99.

30. Ivanell S, Mikkelsen R, Sørensen J, Henningson D. Validation of methods using EllipSys3d. *Tech. Rep*, KTH Engineering Sciences; 2008.

31. Ta Phuoc L. Modèles de sous maille appliqués aux écoulements instationnaires décollés. *Tech. Rep.* France: LIMSI; 1994. LIMSI 93074.

32. Sagaut P. *Large Eddy Simulation for Incompressible Flow.* Berlin Heidelberg: Springer; 2006.

33. Troldborg N, Gaunaa M, Mikkelsen R. Actuator disc simulations of influence of wind shear on power production of wind turbines. In: Proceeding of The science of making torque from wind; 2010:271-297.

34. Eriksson O, Mikkelsen R, Hansen K, Nilsson K, Ivanell S. Analysis of long distance wakes of Horns Rev I using actuator disc approach. *J Phys Conf Ser.* 2014:555. https://doi.org/10.1088/1742-6596/555/1/012032